RESEARCH ARTICLE

Macromolecular Materials and Engineering
Open Access
www.mame-journal.de

Manufacturing and Biological Potential of Saliva-Loaded Core-Sheath Pressure-Spun Polymeric Fibers

*Vansh Thukral, Nanang Qosim, Andre Kurniawan, Merve Gültekinoğlu, H.M. Thushari U. Herath, Gareth R. Williams, and Mohan Edirisinghe**

The rich array of antimicrobial components in saliva offers alternative treatments for drug-resistant bacteria. One therapeutic challenge associated with the effective delivery of salivary components is the quick degradation of salivary proteins outside the oral environment. In this study, polyethylene oxide (sheath) and polycaprolactone (core) based fibers are successfully synthesized using the pressurized gyration technique. Six different pressure-spun fibers are produced. These fibers are created by varying the quantity of artificial saliva in the sheath layer. This unique and effective methodology of embedding saliva within the sheath of the fiber exhibits enhanced bacterial inhibition against *Escherichia coli* and *Staphylococcus aureus* with 80% and 78% inhibition efficiency, respectively. This study showcases a novel technique for promoting wound healing, utilizing core-sheath fibers, which have tremendous potential because of their superior antimicrobial properties, while also aiding in the process of epithelialization. In vitro, cytotoxicity test results showed that there is no cytotoxic effect on the fibroblast cell line. As a result, it is evaluated that the produced fiber meshes can be ideal wound dressing material, considering their lack of toxic effects and high antibacterial activity levels.

1. Introduction

Wound infections remain a significant clinical challenge, requiring innovative approaches to improve healing outcomes and prevent complications. These challenges necessitate the development of advanced wound dressings that not only prevent infections but also actively promote tissue regeneration. Core-sheath polymeric fibers have emerged as promising candidates for such applications, offering advantages such as tunable structural properties, controlled therapeutic agent release, and biocompatibility.[1–3] Additionally, the nanofiber meshes resemble the physical extracellular matrix of the skin, providing a supporting environment for cell growth and wound healing.[4–6] The invention of the core-sheath nanofiber structure with core polymer encased within the sheath polymer allows drug release directly to the wound site.[7] The production of nanofibers using electrospinning,[8–10] interfacial polymerization,[11,12] template synthesis,[13,14] melt extrusion,[15,16] and pressurized gyration[17,18] opened new avenues for their potential application in wound dressing. The higher production rate, scalability, versatility in material selection, enhanced control over fiber morphology, and simpler equipment with lower operational costs are some of the key

V. Thukral, N. Qosim, M. Edirisinghe
Department of Mechanical Engineering
University College London
London WC1E 7JE, UK
E-mail: m.edirisinghe@ucl.ac.uk

N. Qosim
Department of Mechanical Engineering
Politeknik Negeri Malang
Jl. Soekarno Hatta No. 9, Malang, Jawa Timur 65141, Indonesia

A. Kurniawan
Department of Mechanical Engineering
Faculty of Engineering
Universitas Negeri Padang
Jl. Prof. Dr. Hamka, Air Tawar, Padang, Sumatera Barat 25131, Indonesia

M. Gültekinoğlu
Department of Nanotechnology & Nanomedicine
Institute for Graduate Studies in Science & Engineering
Hacettepe University
Ankara 06800, Turkey

H. T. U. Herath
Department of Medical Laboratory Science
Faculty of Allied Health Sciences
University of Peradeniya
Peradeniya 20400, Sri Lanka

G. R. Williams
UCL School of Pharmacy
University College London
29–39 Brunswick Square, London WC1N 1AX, UK

The ORCID identification number(s) for the author(s) of this article can be found under https://doi.org/10.1002/mame.202400403

DOI: 10.1002/mame.202400403

Table 1. Viscosity and surface tension of solutions used in the study.

Solution	Quantity of saliva [mL]	Viscosity [mPa s]	Surface tension [mN m^{-1}]
Artificial saliva	–	8 ± 0.6	64 ± 2
PCL	–	5280 ± 80	27 ± 2
PEO	–	23460 ± 220	58 ± 5
PEO	0.5	22730 ± 240	56 ± 4
PEO	1	20650 ± 210	56 ± 3
PEO	2	15320 ± 120	54 ± 2

features demonstrated by the pressurized gyration spinning technique,[19–21] which are well-suited for the generation of core-sheath fibers over the other techniques.

Through careful selection of core and sheath materials and optimizing the fabrication process, core-sheath fibers can be designed to overcome the complex needs of different wound types.[22] Polyethylene oxide (PEO) offers hydrophilicity, biocompatibility, non-toxicity, mechanical strength, and stable degradation products, making it an ideal material for forming a flexible and strong outer sheath layer in core-sheath fibers. Additionally, it is a highly water soluble polymer that can accelerate drug release and support cell proliferation.[3,23,24] The choice of polycaprolactone (PCL) as the inner core material in core-sheath fibers offers attractive properties such as prolonged biodegradability, relatively high mechanical and tensile strength as well as biocompatibility along with non-toxic, less acidic degradation products.[25–28] Therefore, the PCL/PEO core-sheath fibers have the potential to be an excellent carrier medium for efficient encapsulation of drugs for accelerated wound recovery.

While many studies have focused on synthetic antimicrobial agents or metallic nanoparticles in wound dressings, there is limited research on utilizing natural therapeutic agents like saliva for broader wound healing applications. Saliva has established itself as an excellent natural antimicrobial agent, controlling the growth of microorganisms in the mouth, protecting against infections, and maintaining a balanced oral microbiome.[29,30] The presence of abundant antimicrobial, antifungal, and antibacterial components in saliva, such as lysozyme, lactoferrin, histatins, defensins, peroxidase systems, immunoglobulins, mucins, and growth factors, plays a key role in accelerating the healing of oral wounds.[31,32] Despite its therapeutic potential, its instability outside the oral environment has restricted its broader application. To address this limitation, encapsulating saliva within a protective matrix, such as core-sheath fibers, offers a novel method to stabilize and deliver its bioactive components effectively.

The delivery of salivary components using core-sheath fibers for targeted wound healing has not been studied to date. This study explores the development of artificial saliva-loaded core-sheath fibers using the pressurized gyration technique, aiming to leverage saliva's inherent therapeutic properties for wound care. By varying the quantity of artificial saliva in the sheath layer, we fabricated different fiber compositions and systematically evaluated their antibacterial activity, biocompatibility, and structural properties. This work represents the first effort to integrate artificial saliva into nanofiber technology, providing a biocompatible, non-toxic, and degradable wound dressing material with enhanced antibacterial efficacy. By combining saliva's bioactivity with the structural benefits of core-sheath fibers, this research introduces a promising approach to advancing wound healing technologies.

2. Experimental Section

2.1. Materials

Polycaprolactone (PCL; $M_W = 80\,000$), poly(ethylene oxide) (PEO; $M_W = 200\,000$), magnesium chloride (MgCl), sodium bicarbonate, collagen solution (from calf skin), lactoferrin (from human milk), curcumin (from *Curcuma longa*), calcium chloride ($CaCl_2$), phosphate-buffered saline (PBS; pH 7.4), glutaraldehyde (25% water solution), dimethyl sulfoxide (DMSO), MTT (3-(4,5-dimethylthiazol-2-yl)-2,5-diphenyltetrazolium bromide), Dulbecco's modified Eagle's medium (DMEM), fetal bovine serum (FBS), L-glutamine, penicillin/streptomycin, and Luria-Bertani medium were purchased from Sigma–Aldrich, (Gillingham, UK).

2.2. Custom-Made Artificial Saliva Composition

The artificial saliva solution was formulated using 200 mL of deionized (DI) water and adding 0.04 g of ccalcium chloride. Then, 0.02 g of magnesium chloride was mixed in the above-prepared solution. The stock formulation was accomplished by adding 0.3 g of sodium bicarbonate and stirring using a magnetic stirrer (MS7-H550-Pro, DLAB, Beijing, China) at a rotation speed of 240 RPM till all the salts were completely dissolved. In the above-prepared stock, the bioactive ingredients were sequentially and slowly mixed, starting with 5 mg of lactoferrin, which is a glycoprotein that has a high affinity to iron ions and has antibacterial capabilities. Then, 20 mL of a 0.1% collagen solution in 0.1 M acetic acid was added, a fundamental constituent of the extracellular matrix, which plays a crucial role in promoting cell attachment, migration, proliferation, and providing necessary viscosity to the solution. Finally, 1 mg of curcumin was added to the solution. The solution was then left to stir with the help of a magnetic stirrer for 24 h so that all the components could be completely and uniformly dissolved. These salivary components were incorporated into the preparation of artificial saliva solution based on their established presence in the composition of natural human saliva and the documented use of some of these ingredients in previous studies on artificial saliva formulations.[33,34]

2.3. Solution Preparation and Characterization

The sheath solution was prepared using a 40% (w/v) of PEO solution in DI water, and then the artificial saliva solution (0.5, 1, and 2 mL) was added to separate vials containing 10 mL of PEO solutions, respectively. Then, a 15% (w/v) core solution was prepared by dissolving PCL in chloroform. The viscosity and surface tension of all prepared solutions were tested using a DV-III Ultra programmable rheometer (Brookfield Engineering Laboratories Inc, Massachusetts, USA) and a Tensiometer K9 (Kruss GmbH, Hamburg, Germany), respectively. Each measurement was performed three times using calibrated equipment, with the results presented as the mean ± S.D. (**Table 1**).

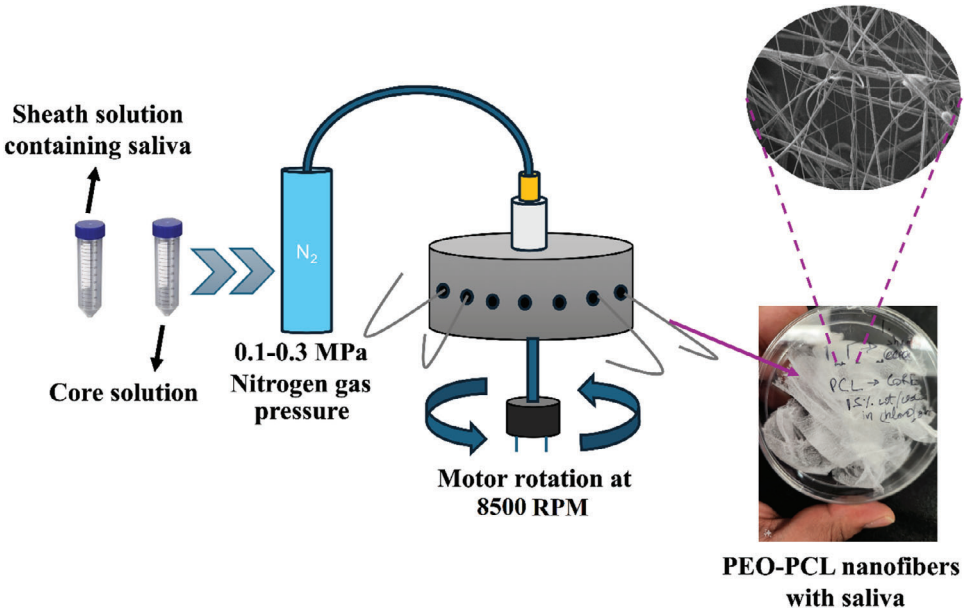

Figure 1. PEO with encapsulated saliva as the sheath and PCL as the core for fiber manufacturing using pressurized gyration.

2.4. Pressurized Gyration for Fiber Production

Figure 1 depicts the schematic diagram of the pressurized gyration technique for the preparation of core-sheath fibers. The spinning vessel was filled with 4 mL of PEO solution into the sheath reservoir, and 4 mL of the PCL solution was fed to the core reservoir. Nitrogen gas at a pressure of 0.1–0.3 MPa was introduced into the core and sheath reservoir through a gas inlet, while the spinning vessel was simultaneously rotated by an adjustable motor at a speed of 8500 RPM. With these parameters, six different fiber samples (**Table 2**) were spun and ejected from the orifices, collected by the rods present at the periphery of the spinning vessel at a 100 mm distance. This spinning process was executed for 30 s under relative humidity and temperature of 54% and 16 °C, respectively.

2.5. Fiber Characterizations

2.5.1. Fourier Transform Infrared Spectroscopy

Approx 5 mg fibers from each sample were placed on the ATR crystal of the Fourier Transform Infrared (FTIR) Spectrometer (Nicolet iS50, Thermo Scientific, Waltham, USA), and then the spectra were recorded by analyzing the samples in the wavenumber range (4000–400 cm^{-1}) with a resolution of 4 cm^{-1}. The ATR crystal was cleaned gently with isopropanol after each spectrum and was dried completely before the next sample measurement.

Table 2. Parameters used to generate different core-sheath fibers.

Sample number	Gas pressure [MPa]	Quantity of saliva [mL]
F1	0.2	–
F2	0.2	0.5
F3	0.1	0.5
F4	0.3	0.5
F5	0.2	1
F6	0.2	2

2.5.2. Scanning Electron Microscopy

The fibers spun at different gas pressures and different saliva percentages were observed using a scanning electron microscope (SEM, Gemini 360, Carl Zeiss Microscopy GmbH, Germany). High-resolution SEM imaging was performed with an acceleration voltage of 1 kV. The fiber size distribution and average fiber diameter were analyzed from the SEM images using a Java-based image processing software, ImageJ. To evaluate the above-mentioned metrics of the fibers, 100 fiber strands were randomly selected, and the histogram of the fiber size was plotted using Origin Pro software.

2.5.3. Artificial Saliva Encapsulation and In-Vitro Release Study

For in-vitro saliva release measurement, PBS was used as an appropriate test medium. The artificial saliva was released in the PBS solution, and its concentration was assessed using UV–Vis (Jenway 7315, Cole-Parmer Ltd., St. Neots, UK) spectroscopy at a wavelength of 218 nm. Before conducting the release performance, a calibration curve was plotted for 0.1–1 mg mL^{-1} of artificial saliva solution concentrations. The release study of the artificial saliva was carried out in 20 mL of PBS solution and incubated in a shaker at 37 °C. After 5, 10, 15, 30, and 60 min time intervals, 3 mL of the resultant PBS solution was taken for release profile analysis and was replaced by 3 mL of the fresh PBS solution stock. These 3 mL removed supernatant solutions were

further assessed using a UV–Vis spectrophotometer. The UV–Vis spectrophotometer provided the data to further calculate the cumulative saliva release percentage of saliva additive. All the measurements from the UV–Vis spectrometer were taken in triplicate ($n = 3$).

2.5.4. Cytotoxicity Study

Fibrous samples were tested in terms of direct cell cytotoxicity/viability (according to ISO 10993–5). L929 (ATCC-NCTC clone 929:CCL1) mouse fibroblast cell line was used. Six different samples were prepared and sterilized by UV irradiation before the test. MTT (3-(4,5-dimethylthiazol-2-yl)-2,5-diphenyltetrazolium bromide) assay was performed.[35] Cell cytotoxicity was determined through cell viability percentage by colorimetric analysis of the mitochondrial activities of cells. The cell culture medium consisted of 90% DMEM, 10% FBS, 2 mM L-glutamine, and 100 IU/mL penicillin/streptomycin. The cells' incubation conditions were kept constant at 37 °C, 5% CO_2, and 95% relative humidity. The cells were prepared at 1×10^5 cells mL^{-1} concentration and the 100 µL cell suspension (1×10^4 cells to each well) was seeded to each well at 96 well plates. The cell culture media was used as a negative control, and the 10% DMSO-90% medium was used as a toxic positive control. After the 24 h incubation period, the culture medium was replaced by 100 µL culture medium with 10% MTT solution and incubated at 37 °C for 240 min. Then, the medium was replaced by 100 µL of DMSO to dissolve formazan crystals for 30 min. The 96-well plate ($n = 3$) was measured at 575 nm absorbance by ELISA plate reader (SpectroStar nano, BMG Labtech, Ortenberg, Germany).

2.5.5. Antibacterial Activity

Antimicrobial activities of the core-sheath fiber samples against gram-positive *Staphylococcus aureus* (*S. aureus*, ATCC #29 213) and gram-negative *Escherichia coli* (*E. coli*, ATCC #25922) bacteria strains were used to determine the antibacterial activity by bacterial adhesion. The bacterial solution (Luria-Bertani medium, Sigma, #L7275) was adjusted to 0.4 optical density (OD) and directly used. The samples were prepared into a 48-well polystyrene plate and sterilized by UV irradiation for 1 h. 0.5 mL bacteria suspension was added to each well. The samples were incubated for 4 h at 37 °C. After 4 h, samples were immersed in 1 mL PBS (Sigma Aldrich, #P4417) solution in 2 mL sterile test tubes and ultrasonicated for 15 min. 150 µL samples were collected from each of the samples in a 96-well plate. Then, OD was measured in a 96-well plate at 600 nm absorbance by ELISA plate reader ($n = 3$). Bacteria solution and PBS absorbance were also measured as control and blank groups, respectively. The bacterial inhibition percentage was calculated by the following equation:

$$\text{Bacterial inhibition } \% = \left(\frac{A_c - A_s}{A_c}\right) \chi\, 100 \quad (1)$$

where A_C and A_S represent the average optical density values of the control group and the sample group, respectively. Additionally, after the incubation period, glutaraldehyde fixation was performed, and the water content was removed by serial alcohol dilutions. Prior to analysis, samples were coated with conductive carbon and visualized by SEM.

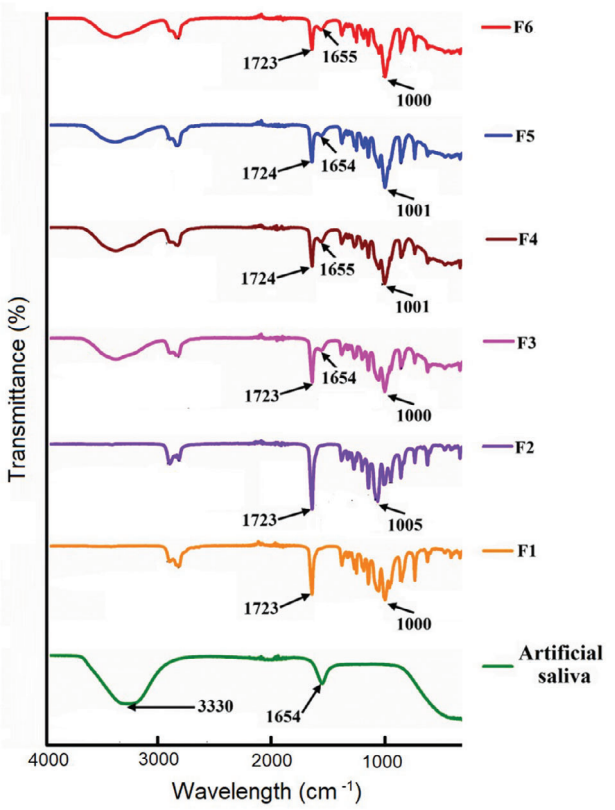

Figure 2. FTIR spectra of artificial saliva and all core-sheath pressure-spun fiber samples.

3. Results and Discussion

3.1. Fiber Composition

FTIR spectroscopy analysis was conducted to further investigate the presence of all components in the fibers produced. As shown in **Figure 2**, the FTIR spectrum of the artificial saliva displayed a broad peak at 3330 cm^{-1}. The broad peak at 3330 cm^{-1} is assigned to the stretching vibration of O—H due to the fact that there is a substantial amount of water present in the artificial saliva. The saliva spectrum closely mirrors that of water, with other components present in lesser amounts, thereby making water the predominant element in the spectrum. The core-sheath fiber sample without the addition of artificial saliva presented the characteristic vibration peaks for PEO as well as PCL fibers. The 1000–1005 cm^{-1} vibration peak was assigned to molecular stretching due to C—O—C stretching ether group of the PEO sheath.[36] Whereas the PCL core vibration FTIR peak was observed at 1723–1724 cm^{-1}, indicating the presence of sharp C═O characteristic bands.[36] For the saliva-loaded fiber samples, the characteristics peaks of O—H hydroxyl vibration peaks appeared strongly with the increase in the artificial saliva dosage along with the vibration peaks of PCL and PEO fibers. Thus, the successful

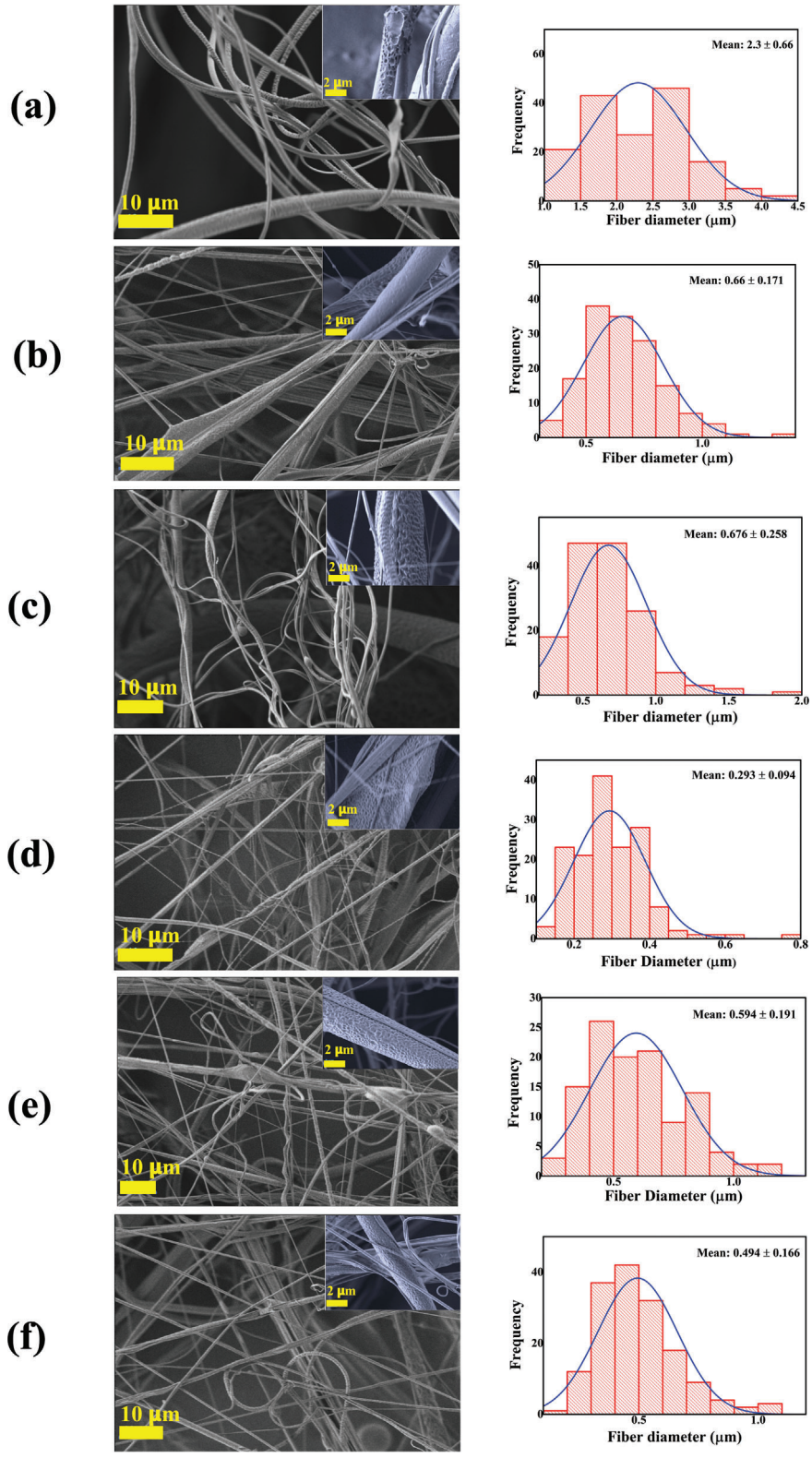

Figure 3. Scanning electron micrographs of all samples, together with their size distributions: a). F1; b). F2; c). F3; d). F4; e). F5; and f). F6. (inset micrographs show a magnified image of the fiber).

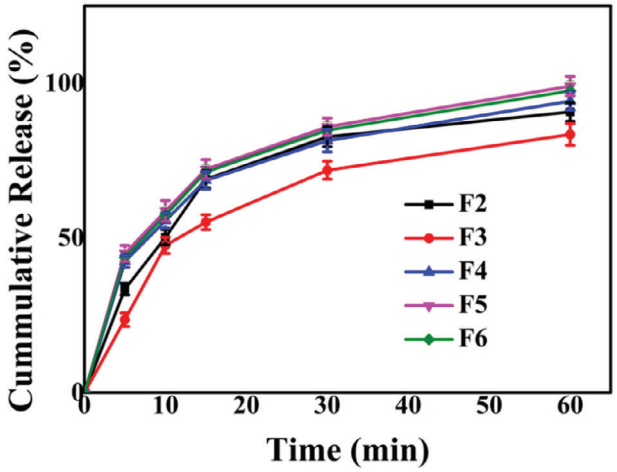

Figure 4. Cumulative release of saliva loaded in core-sheath fibers.

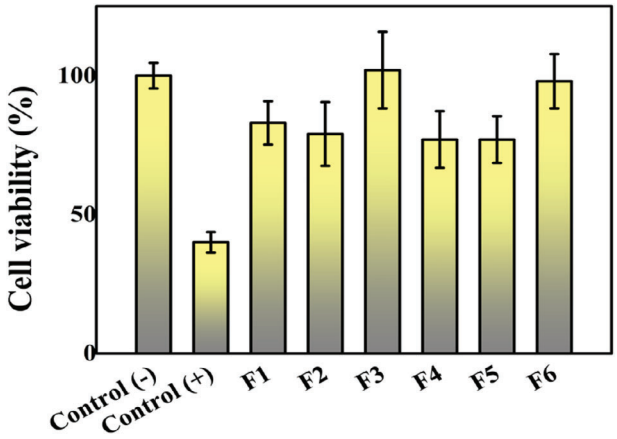

Figure 5. Cell viability test for cell culture media as the negative control, 10% DMSO-90% medium as the positive toxic control. (Arithmetic means, error bars represent 95% confidence intervals).

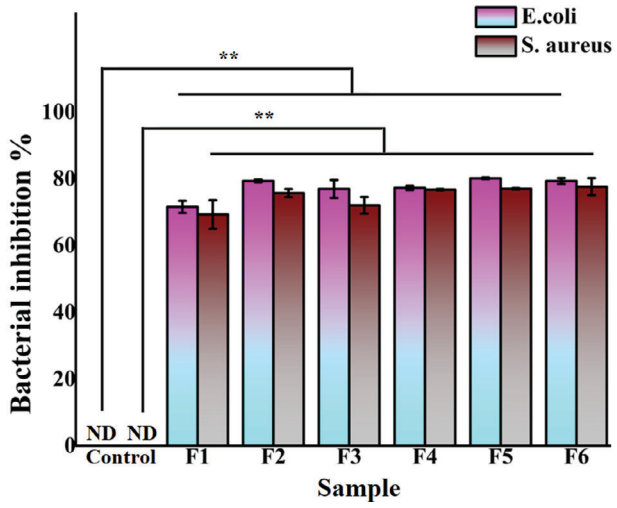

Figure 6. Antibacterial test results of saliva-loaded core-sheath fiber meshes with bacterial inhibition percentage against *gram-negative E. coli* and *gram-positive S. aureus* bacteria species. $^{**}p$-value ≤ 0.005. ND = not detected.

encapsulation of artificial saliva in the core-sheath pressure-spun fiber matrix was confirmed.

3.2. Morphology and Size Distribution

All the polymer solutions were successfully spun using pressurized gyration. **Figure 3** represents the morphology of the as-prepared fibers with different spinning parameters. For each fiber, a histogram of the fiber diameter was plotted, and the normal distribution of the histogram was found to statistically determine the degree of variations in the fiber size. The 40% (w/v solution of PEO in DI water, along with 15% w/v PCL in chloroform solution, was spun at 0.2 MPa nitrogen pressure, resulting in fibers with a diameter of 2.3 μm. The fiber produced without the incorporation of saliva in the PEO solution caused thicker fibers to be developed (as shown in Figure 3a). This is because the PEO solution without the addition of saliva has a higher viscosity than after its addition, as shown in Table 1. In the process of pressurized gyration, a more viscous solution has higher resistance to flow and deformation. When the polymer solution is spun under high pressure in the gyration process, the viscous forces oppose the stretching of the polymer jet. This means that the solution does not elongate as much, resulting in thicker fibers. Additionally, high-viscosity solutions tend to have slower solvent evaporation rates during the fiber formation process. This further contributes to larger fiber diameters, as the fibers maintain their thickness before the solvent evaporates completely.[8,37]

When 0.5 mL of saliva was mixed in the PEO solution with a varied gas pressure of 0.1–0.3 MPa, the 0.2 MPa gas pressure generated 660 nm fibers (Figure 3b) while 0.1 MPa gas pressure led to the generation of 676 nm range fiber (Figure 3c) and 0.3 MPa gas pressure produced 293 nm fibers (Figure 3d). With the same parameters, the addition of saliva resulted in a decrease in fiber diameter (Figure 3e,f). Thus, a higher gas pressure applied to the pressurized gyration vessel produces finer fibers.[8,38,39] Further, the inset micrograph of the SEM images reveals the presence of nanopores on the surface of all samples, which tends to boost the release kinetics of the encapsulated saliva.[40–42]

3.3. In-Vitro Artificial Saliva Release

The in-vitro artificial saliva release profile from the core-sheath fibers was characterized by an initial burst release profile followed by a more sustained release phase after 5 min (**Figure 4**). The initial burst release, accounting for ≈34–48% of the total artificial saliva content for all fiber samples (F2-F6), could be attributed to the rapid dissolution of the PEO sheath within the PBS solution mainly due to the hydrophilic nature of PEO. Following the initial burst, the release rate gradually decreases, suggesting a high initial availability of artificial saliva components in the PEO sheath. Over time, the release rate further diminishes due to the gradual reduction in the remaining amount of artificial saliva.

A total saliva release of ≈99% was observed for the ultrafine fiber (F4) with a 293 nm diameter within a time period of 60 min, which aligns well with literature indicating that finer diameters result in faster release rates, while sample F3 exhibited the slowest release of artificial saliva at 78%, likely due to its larger fiber

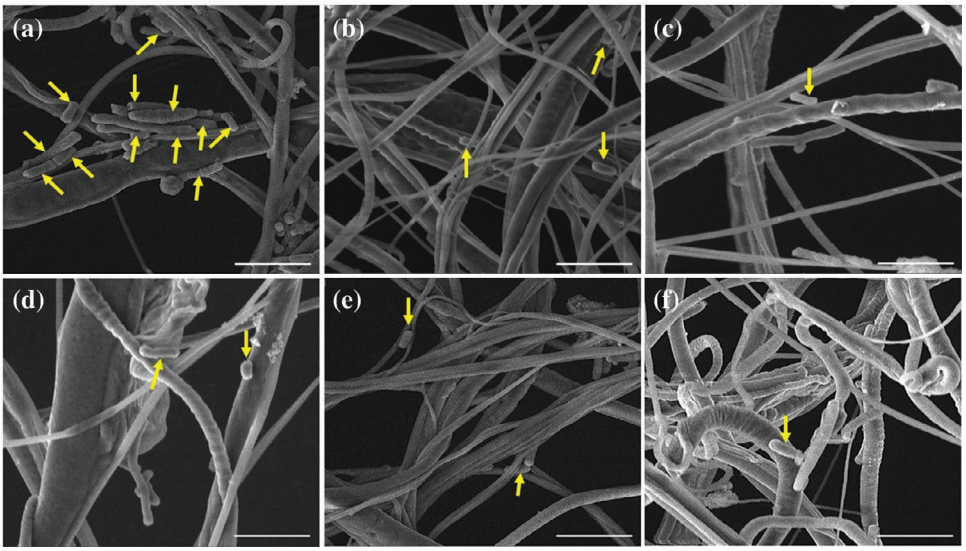

Figure 7. SEM micrographs of saliva-loaded core-shell fiber meshes after incubation with *gram-negative E. coli* bacteria a) F1, b) F2, c) F3, d) F4, e) F5, and f) F6. (Scale bar = 5 µm).

diameter of 676 nm compared to the other fiber samples. This release profile could be highly beneficial for wounds, such as burns or complex injuries, that demand swift and effective treatment to prevent infection and promote healing. The artificial saliva formulation, prepared in DI water, resulted in the rapid dissolution of the fibers in an aqueous medium (PBS), offering an accelerated drug release that is advantageous for wound management by delivering an immediate therapeutic effect to inhibit microbial activity.[43] This rapid release of artificial saliva is particularly critical during the early stages of wound management, as it helps reduce the risk of infection, potentially lowers the required doses of oral antibiotics, and facilitates the initial phases of healing and tissue repair.[44,45]

3.4. Cytotoxicity

Mouse fibroblast cell line (L929) was used to assess the fiber samples to evaluate the negative side effects or cytotoxicity to the surrounding tissues when used as a natural wound dressing in drug delivery applications. ISO10993-5 "Biological evaluation of medical devices – Part 5, tests for in vitro cytotoxicity: Indirect MTT cytotoxicity" assay was applied to test the fiber samples. The cell viability ratio for the core-sheath fibers loaded with artificial saliva is presented in **Figure 5** and Table S1 (Supporting Information).

Promising results were observed with no cytotoxic effect in any of the fiber samples for the saliva-loaded fibers. The negative control group exhibited perfect cell viability of 100%. 10% DMSO-90% culture media was used as the positive control group. DMSO content reduced cell viability to 50% and confirmed that the cells were not immortal. However, samples F2 and F4, which represented 0.5 mL artificial saliva-loaded core-sheath fibers, presented moderate cell viability of 79% and 77%, respectively. The cell viability results for samples F5 and F6, which represented 1 and 2 mL of artificial saliva-loaded fibers, respectively, showed no cytotoxicity with significant cell viability. F5 demonstrated 77% cell viability, while F6 exceeded 100%, suggesting enhanced cell growth, particularly for the 2 mL saliva-loaded fibers (F6). According to the applied ISO10993-5 standard, above 70% cell viability is approved as non-toxic materials. In the present study, all the sample groups exhibited cell viability above 70%. The pressure-spun fiber formulations, especially for F3 and F6, demonstrated the highest cell viability and were suitable for wound healing applications without any side effects to the surrounding dermal tissues.

3.5. Antibacterial Activity

The antibacterial activity of the core-sheath fibers was analyzed using the bacterial adhesion capability for biofilm generation. Test results (**Figure 6**) indicated that increasing the volume of artificial saliva added to the fiber enhanced bacterial inhibition. The antibacterial activity was tested against two bacterial strains, gram-negative *E. coli*, and gram-positive *S. aureus* bacteria species. As shown in Table S2 (Supporting Information), all the fiber samples displayed significant antibacterial activity against *E. coli*, and the inhibition percentages varied between 72–80%. The 1 mL saliva-embedded fiber sample (F5) exhibited strong antibacterial effects, achieving the highest inhibition rate of 80% against *E. coli*. Furthermore, all samples demonstrated substantial antibacterial activity against *S. aureus*, with inhibition percentages ranging from 69% to 78%. The highest *S. aureus* inhibition percentage was observed in the 2 mL saliva-loaded fiber sample (F6), which demonstrated 78% inhibition, emphasizing its potent antibacterial properties. The test results clearly indicate that increased loading of artificial saliva in the fibers significantly boosted their antibacterial activity.

Additionally, bacterial adherence on fiber meshes was investigated by SEM. **Figures 7** and **8** show the antibacterial activity of fiber meshes by SEM images for *E. coli* and *S. aureus*, respectively. The SEM micrographs support the bacterial adherence

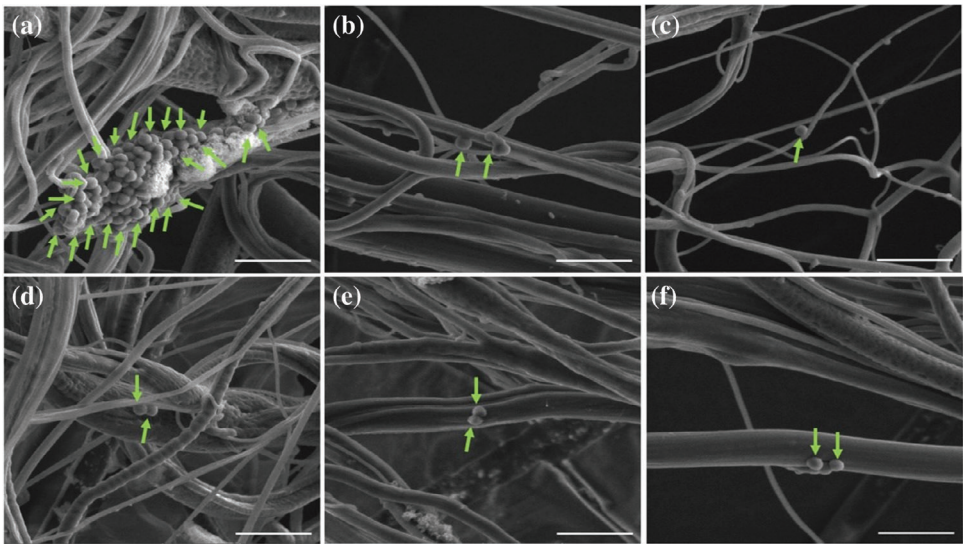

Figure 8. SEM micrographs of saliva-loaded core-shell fiber meshes after incubation with *gram-positive S. aureus* bacteria a) F1, b) F2, c) F3, d) F4, e) F5, and f) F6. (Scale bar = 5 µm).

test results. Null-fiber samples (F1) showed a higher number of bacteria adhered on the surface for both *E. coli* and *S. aureus* bacteria species. In Figure 7A, *E. coli* bacteria have larger sizes that depict cell division according to whether they are in the doubling phase. In Figure 8A, F1 samples exhibited a thick accumulated bacteria layer. On the contrary, increasing saliva content reduced the adhesion of bacteria to the fibers for both *E. coli* and *S. aureus* bacteria species. Superior antibacterial activity against both bacterial strains further suggests the effectiveness of these saliva-loaded fibers in combating a broad spectrum of pathogens, which is crucial for wound healing applications where mixed infections are common.

4. Conclusions

The study effectively showcased the production and assessment of saliva-blended core-sheath fibers using PEO as the outer layer and PCL as the inner material. The innovative method of integrating synthetic saliva into fibers using a pressurized gyration process demonstrated encouraging outcomes in terms of antibacterial effectiveness and potential for treating wounds. The samples included with artificial saliva exhibited notable antibacterial characteristics, with inhibitory effectiveness of 80% against *E. coli* and 78% against *S. aureus*. This indicates a potent efficacy against both *gram-negative* and *gram-positive* bacteria. SEM micrographs showed that different gas pressures used in the pressurized gyration process had an impact on the shape and size of the fibers. Higher gas pressure led to the production of thinner fibers, which in turn improved the surface structure and increased the speed at which the enclosed saliva was released. Significantly, fibers of ≈293 nm in diameter demonstrated a rapid discharge of saliva, accomplishing over 99% complete release within 1 h. This characteristic is beneficial for promptly obtaining therapeutic benefits in wound treatment. Cytotoxicity assays further confirmed the biocompatibility of the fibers, with those containing higher saliva content exhibiting significant cell viability, underscoring their potential for biomedical applications. While the current study focused on the initial 4-h antibacterial performance to highlight the fibers' immediate efficacy, we recognize the importance of evaluating long-term antibacterial properties, especially for applications requiring sustained protection. Future research will prioritize extending the antibacterial testing period to provide a more comprehensive understanding of the fibers' long-term efficacy. Additionally, exploring the use of natural saliva, even though it will be very challenging and require numerous studies as natural saliva is unique to each individual, remains an important avenue for future studies. This work sets the stage for further advancements in the development of innovative wound dressing materials.

Supporting Information

Supporting Information is available from the Wiley Online Library or from the author.

Acknowledgements

V.T. and N.Q. Contributed equally to this work. N.Q. thanks LPDP, The Ministry of Finance, The Republic of Indonesia, for providing a scholarship for his doctoral studies at UCL. The support from the UK Engineering and Physical Sciences Research Council (EPSRC) for advancing pressurized gyration research at UCL is sincerely appreciated (Grants EP/S016872/1, EP/N034228/1, and EP/L023059/1). Special thanks go to Hamta Majd (Department of Mechanical Engineering, UCL) for providing a core-sheath spinning vessel.

Conflict of Interest

The authors declare no conflict of interest.

Data Availability Statement

The data that support the findings of this study are available from the corresponding author upon reasonable request.

Keywords

core-sheath, fibers, polymers, pressure-spinning, pressurized gyration, saliva

Received: October 29, 2024
Revised: December 11, 2024
Published online:

[1] N. Qosim, H. Majd, S. Huo, M. Edirisinghe, G. R. Williams, *Int. J. Pharm.* **2024**, *654*, 123972.
[2] C. Li, Z. H. Wang, D. G. Yu, G. R. Williams, *Nanoscale Res. Lett.* **2014**, *9*, 1.
[3] H. Majd, M. Gultekinoglu, C. Bayram, B. Karaosmanoğlu, E. Z. Taşkıran, D. Kart, Ö. D. Erol, A. Harker, M. Edirisinghe, *Macromol. Mater. Eng.* **2024**, *309*, 2400014.
[4] A. Vijayan, N. C. K., G. S. Vinod Kumar, *Nanoscale Adv.* **2021**, *3*, 3085.
[5] L. Sethuram, J. Thomas, *Biomed. Pharmacother.* **2022**, *157*, 113996.
[6] F. Anjum, N. A. Agabalyan, H. D. Sparks, N. L. Rosin, M. S. Kallos, J. Biernaskie, *Sci. Rep.* **2017**, *7*, 1
[7] J. Xue, T. Wu, Y. Dai, Y. Xia, *Chem. Rev.* **2019**, *119*, 5298.
[8] N. Qosim, H. Majd, J. Ahmed, G. Williams, M. Edirisinghe, *Cellulose* **2024**, *31*, 2815.
[9] S. Moon, K. Park, E. Seo, K. J. Lee, *Macromol. Mater. Eng.* **2018**, *303*, 1700565.
[10] Y. Geng, G. R. Williams, *Int. J. Pharm.* **2023**, *648*, 123557.
[11] F. Zhang, J. b. Fan, S. Wang, *Angew. Chem., Int. Ed.* **2020**, *59*, 21840.
[12] H. Guan, L. Z. Fan, H. Zhang, X. Qu, *Electrochim. Acta* **2010**, *56*, 964.
[13] H. W. Liang, Q. F. Guan, L. F. Chen, Z. Zhu, W. J. Zhang, S. H. Yu, *Angew. Chem., Int. Ed.* **2012**, *51*, 5101.
[14] J. Yan, Y. Han, S. Xia, X. Wang, Y. Zhang, J. Yu, B. Ding, *Adv. Funct. Mater.* **2019**, *29*, 1907919.
[15] G. Sui, W. H. Zhong, M. A. Fuqua, C. A. Ulven, *Macromol. Chem. Phys.* **2007**, *208*, 1928.
[16] H. Li, Y. Ke, Y. Hu, *J. Appl. Polym. Sci.* **2006**, *99*, 1018.
[17] S. Mahalingam, S. Huo, S. Homer-Vanniasinkam, M. Edirisinghe, *Polymers* **2020**, *12*, 1709.
[18] H. Alenezi, M. E. Cam, M. Edirisinghe, *Appl. Phys. Rev.* **2021**, *8*, 041412.
[19] Y. Dai, M. Edirisinghe, *Expert Opin. Drug Deliv.* **2024**, *21*, 1683.
[20] N. Qosim, Y. Dai, G. R. Williams, M. Edirisinghe, *Int. Mater. Rev.* **2024**, *69*, 309.
[21] A. M. Klein, N. Qosim, G. Williams, M. Edirisinghe, R. K. Matharu, *Pharmaceutics* **2024**, *16*, 1066.
[22] J. Ahmed, M. Gultekinoglu, M. Edirisinghe, *Wiley Interdiscip. Rev. Nanomed. Nanobiotechnol.* **2024**, *16*, e1916.
[23] E. Maccaferri, J. Ortolani, L. Mazzocchetti, T. Benelli, T. M. Brugo, A. Zucchelli, L. Giorgini, *ACS Omega* **2022**, *7*, 23189.
[24] Y. C. Jung, H. Muramatsu, K. C. Park, D. Shimamoto, J. H. Kim, T. Hayashi, S. M. Song, Y. A. Kim, M. Endo, M. S. Dresselhaus, *Macromol. Rapid. Com.* **2009**, *30*, 2084.
[25] A. Azari, A. Golchin, M. M. Maymand, F. Mansouri, A. Ardeshirylajimi, *Adv. Pharm. Bull.* **2022**, *12*, 4.
[26] C. Qian, Y. Liu, S. Chen, C. Zhang, X. Chen, Y. Liu, P. Liu, *Front. Bioeng. Biotechnol.* **2023**, *11*, 1205252.
[27] T. H. Tabane, B. S. Batlokwa, *J. Drug Deliv. Ther.* **2023**, *13*, 91.
[28] T. C. Mokhena, M. B. Chabalala, S. Mapukata, A. Mtibe, L. Hlekelele, Z. Cele, M. J. Mochane, B. Ntsendwana, T. A. Nhlapo, T. P. Mokoena, M. F. Bambo, K. P. Matabola, S. S. Ray, E. R. Sadiku, K. Shingange, *Macromol. Mater. Eng.* **2024**, *309*, 2300388.
[29] A. M. Lynge Pedersen, D. Belstrøm, *J. Dent.* **2019**, *80*, S3.
[30] T. Vila, A. M. Rizk, A. S. Sultan, M. A. Jabra-Rizk, *PLoS Pathog.* **2019**, *15*, e1008058.
[31] G. N. Güncü, D. Yilmaz, E. Könönen, U. K. Gürsoy, *Front. Cell. Infect. Microbiol.* **2015**, *5*, e1008058.
[32] T. Zhang, W. An, J. Sun, F. Duan, Z. Shao, F. Zhang, T. Jiang, X. Deng, C. Boyer, W. Gao, *Nano Lett.* **2022**, *22*, 8294.
[33] R. Mungia, S. M. Cano, D. A. Johnson, H. Dang, J. P. Brown, *Aging Clin. Exp. Res.* **2008**, *20*, 503.
[34] J. Y. Gal, Y. Fovet, M. Adib-Yadzi, *Talanta* **2001**, *53*, 1103.
[35] I. Eroglu, M. Gultekinoglu, C. Bayram, A. Erikci, S. Y. Ciftci, E. Ayse Aksoy, K. Ulubayram, *Pharm. Dev. Technol.* **2019**, *24*, 1144.
[36] A. Afshar, H. Majd, A. Harker, M. Edirisinghe, *J. Drug Deliv. Sci. Tec.* **2024**, *95*, 105582.
[37] Y. Dai, J. Ahmed, M. Edirisinghe, *Macromol. Mater. Eng.* **2023**, *308*, 2300033.
[38] P. L. Heseltine, J. Ahmed, M. Edirisinghe, *Macromol. Mater. Eng.* **2018**, *303*, 1800218.
[39] H. Alenezi, M. E. Cam, M. Edirisinghe, *Appl. Phys. Rev.* **2019**, *6*, 041401.
[40] P. Shivanand, O. L. Sprockel, *Int. J. Pharm.* **1998**, *167*, 83.
[41] B. Zhang, A. Gleadall, P. Belton, T. McDonagh, R. Bibb, S. Qi, *Addit. Manuf.* **2021**, *46*, 102196.
[42] F. J. H. Abadi, M. A. Tehran, F. Zamani, M. Nematollahi, L. G. Mobarakeh, M. H. Nasr-Esfahani, *Int. J. Polym. Mater. Po.* **2013**, *63*, 57.
[43] R. Tiwari, K. Pathak, *Pharmaceutics* **2023**, *15*, 634.
[44] B. R. Freedman, C. Hwang, S. Talbot, B. Hibler, S. Matoori, D. J. Mooney, *Sci. Adv.* **2023**, *9*, 20.
[45] S. Saghazadeh, C. Rinoldi, M. Schot, S. S. Kashaf, F. Sharifi, E. Jalilian, K. Nuutila, G. Giatsidis, P. Mostafalu, H. Derakhshandeh, K. Yue, W. Swieszkowski, A. Memic, A. Tamayol, A. Khademhosseini, *Adv. Drug Delivery Rev.* **2018**, *127*, 138.